Acta Polytechnica CTU Proceedings **41**:89–97, 2023
https://doi.org/10.14311/APP.2023.41.0089

Published by the Czech Technical University in Prague

EXPERIMENTAL EVALUATION OF ALUMINOTHERMIC WELDS

Lukáš Zeman[a,*], Jaroslav Valach[a], Petr Zlámal[a], Nela Krčmářová[a], Veronika Koudelková[b], Jaroslav Zeman[c]

[a] *Czech Technical University in Prague, Faculty of Transportation Sciences, Department of Mechanics and Materials, Na Florenci 25, 110 00 Prague 1, Czech Republic*

[b] *Czech Academy of Sciences, Institute of Theoretical and Applied Mechanics, Prosecká 809/76, 190 00 Prague 9, Czech Republic*

[c] *Pandrol CZ, Grupe Delachaux, Jankovcova 938/18a, 170 00 Prague 7, Czech Republic*

[*] corresponding author: zemanl16@cvut.cz

Abstract. The article presents a study of the mechanical processes occurring during the aluminothermic reaction using experimental methods (strain gauges, digital image correlation, thermography, scanning electron microscopy, profilometry). The aluminothermic reaction is a highly efficient welding method due to its exothermic behaviour, however, it places considerable demands not only on the welding technique, but also on the capabilities of the experimental methods used; these limitations are also discussed in the article. The aluminothermic reaction is associated with the formation of a localised heat source with a time evolution dictated by the technological procedure, which manifests itself in heat propagation to the surrounding weld material. The unequal evolution of the temperature field is the fundamental cause of the appearance of the heat affected zone or local deformations or surface curvature, which was the focus of the experimental methods deployed above and the results of which are shown in the article.

Keywords: Aluminothermic reaction, strain gauges, hardness, profilometry, scanning electron microscope.

1. Introduction

In recent years, the welding process has focused on lowering the human factor and increasing the weld joint quality. The resulting material properties depend on the technological process of welding. Production/formation conditions and operating conditions determine the lifetime and the rate of the degradation [1]. For this reason, it is necessary to experimentally observe this process and subsequently evaluate the significant mechanical properties. The welding process is a technology that is widely used in many applications (automotive industry, civil engineering, aerospace, etc.), especially in the case of aerospace, reliability and the associated reduction of the human factor are crucial [2].

The aluminothermic (AT) reaction is a promising welding method used for welding rails, joining ground wires and in the construction of guideways for warehouse stackers. The advantage of the AT welding technology over the commonly used riveting method is that the resulting joint has mechanical properties similar to those of the original element. Moreover, in a riveted connection, a hole is formed in the profile which can initialise defects in the structures and, thus, affect the lifetime of the structure or joint. This supports the idea of applying the AT welding technology within the aerospace field in the case of repairing a defective wing spar for example. AT welding has its own qualities in terms of the mechanical properties of the resulting weld, including the distribution of the heat field throughout the profile [3]. This makes the AT welding method better in its weld quality compared to [4, 5]. Moreover, the Flash Butt Welding (FBW) method has a disadvantage in the form of a softer weld compared to basic materials, whereas the Metal Inert Gas/Metal Active Gas (MIG/MAG) method is strongly dependent on the human factor (the welder's experience). The AT method has a low human factor incidence rate with regards to the appearance of defects in the weld, this fact was now confirmed by the company SSI Schäfer, which replaced the MIG/MAG method with the AT method at the beginning of year 2022, thus, reducing the influence of the human factor by more than 50 % (non-public study of Pandrol CZ).

To increase the reliability of the welded connection and to understand the welding process itself, it is necessary to use suitable experimental methods for the evaluation of the mechanical properties of the welding structure (weld, affected zone, etc.). Here, contact (e.g., strain measurements using strain gauges [6]) and non-contact methods (e.g., optical strain measurements using thermal imaging, laser triangulation inspection [7]) can be used for the observation and evaluation of the welding process [8]. In addition to these macro-level methods, micro-level methods, such as the hardness method or the scanning electron microscopy technique can be performed to evaluate the weld-basic material interface quality or to view changes in the material properties in the affected zone [9, 10].

2. Aluminothermic reaction

The aluminothermic reaction process belongs to the field of powder metallurgy. It involves the composition of a combustible batch of metal oxide (with the target alloy) and aluminium, where aluminium is used as a reducing agent. Since the final enthalpy of the product is higher than the enthalpy of the system at the beginning, the overall reaction enthalpy is negative, i.e., a high amount of heat is released during combustion, thus classifying the process as an exothermic reaction. In addition to the heat, the combustion process converts the metal oxide to pure metal, oxygen molecules bind to the aluminium to form alumina, a crystalline compound occurring naturally as a very hard mineral known as corundum. The corundum is lighter than the weld metal, in this case iron or structural steel of two profiles, the HEB140 profile of 11.375 steel and the 60E2 profile of the R350 grade, and, therefore, it separates from the weld metal with the slag and remains on the surface. The basic ferritic exothermic reaction is given by Equation (1).

$$Fe_2O_3 + 2\,Al \rightarrow 2\,Fe + Al_2O_3 \qquad (1)$$

The welding technology consists of igniting the mixture in a ceramic crucible to produce the reaction described above. When the reaction takes place, the fusible plug at the bottom of the crucible is melted and the weld metal is poured into the prepared mould (Figure 1). The shape of the mould is determined by the dimensions of the profiles to be joined. Thus, the slag and corundum can be cast by overflowing outside the mould into the prepared cup, to eliminate the mixture with the weld metal (the process is described more in [11]). In cooperation with the company Pandrol Ltd. (training centre in Kralupy nad Vltavou), the welding process of two different types of profiles (HEB140 and 60E2) were experimentally investigated. The welding of the joined components was carried out at a neutral temperature (for the Czech Republic, in the range from 17 to 23 °C and given by 'Novelizace předpisu SŽDC S3/2 Bezstyková kolej') as this temperature is different for each country, region or area due to the climate of the area [12].

3. Experimental methods

To describe the strain and changes in the structure during the AT process, several experimental methods were used. These methods were chosen with regard to the possibility of obtaining a comprehensive description of the given issue.

3.1. Strain gauge measurement

Contact strain measurements were performed using GE-LM11 (HBM, Germany) foil strain gauges (SGs), sensors with a 6 mm active length in the Wheatstone quarter bridge configuration. The strain signals from the SGs were recorded using the DAQ MGCplus solution (HBM, Germany) with a 1 S/s sample rate. The strain gauges were bonded to the profile (the position of each SG is depicted in the scheme in Figure 2) with an X280 epoxy adhesive (HBM, Germany) in locations where the expected temperature was below 175 °C. This temperature was set as a safety value to keep the SGs functional.

3.2. Digital image correlation (DIC) method

In addition to the SG measurements, the strain evaluation was performed using the DIC technique [14]. Unlike the SGs, this non-contact method enables the measurement of the full-field displacement and strains and/or to define the virtual SGs. An EOS 550D (Canon Inc., Japan) Digital single-lens reflex (DSLR) camera attached with an EF 70–200 mm f/2.8L lens (Canon Inc., Japan) to observe the welding process. A black-and-white stochastic pattern was sprayed on the surface of the welded profile (in the hot section from 50 to 150 mm from the weld axis) to provide better contrast and to make the DIC procedure more precise. An in-house DIC software toolkit was used for the displacement evaluation in the series of images (5202×3467 px image resolution, approx. 28 μm in pixel size) captured during the welding procedure with a sample rate of 0.2 fps [15]. The tracking of this DIC algorithm consists of two steps. In the first step, the correlation is evaluated at the pixel level using template matching employing the Sum of Squared Differences (SSD) method. In the second step, the sub-pixel precision is obtained according to the interpolation using a third-order bivariate spline over the pixel grid. The resulting best match is found based on the minimisation of the bivariate spline using the Limited-memory Broyden–Fletcher–Goldfarb–Shanno (LM-BFGS) algorithm [16].

3.3. Thermal imaging

The experimental set up was complemented with a FLIR SC7600 thermal imaging camera to highlight the rate of the heat input and the overall distribution of the temperature field across the profile. The thermal image acquisition was performed at 115 fps and, due to the technical limitations of the camera, it was necessary to cover the hottest area with a foil strip. The resulting experimental set up capturing the welding process can be seen in Figure 3.

3.4. Profile and hardness measurement

After the welding process, it is necessary to evaluate whether the weldment meets the requirements according to the type of application, with an emphasis on the weld geometry and the hardness distribution over the weldment travel surface. A satisfactory geometry is a flatness that is limitingly close to the absolute plane, according to the S3/2 regulation. There is an overhang tolerance of 0.5 mm along half a metre distance on each side of the weld axis. Profile laser scanning (ScanControl LLT 2800-25, Micro-epsilon,

FIGURE 1. AT process of the PLA (Préchauffage limité) short pre-heating method using an automatic High Flow Preheating (HFP) unit and a one-shot crucible [13].

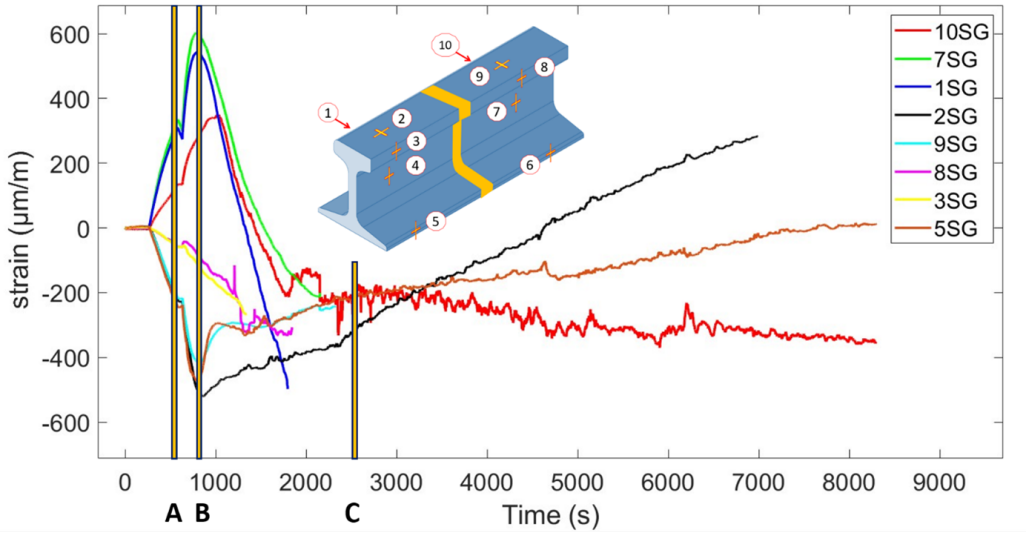

FIGURE 2. Time-strain dependency of the individual SGs. Some of the SG records are missing or shortened due to damage/failed sensor bonding.

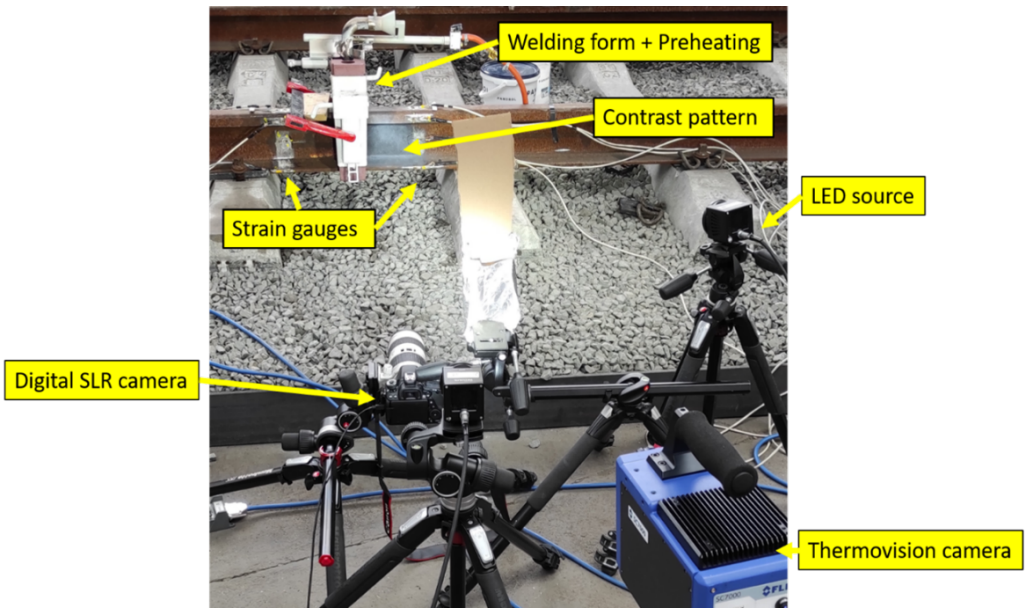

FIGURE 3. Experimental set up for the strain and thermal measurements of the AT welding process.

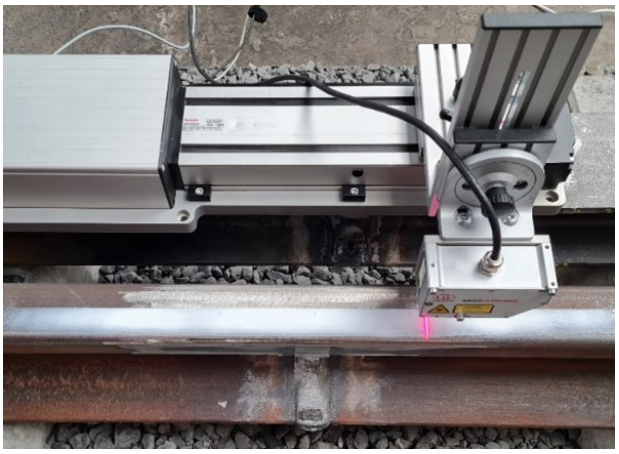

Figure 4. Step-shift laser head assembly for measuring the flatness of the running surface.

USA) based on the laser triangulation method was performed on both profiles (see Figure 4). The preparation of the surface includes polishing the scanning area and a layer of matte white paint to mitigate the frequency of the reflected beam. For the hardness measurements, it is assumed that the hardness value of the weld should be higher than the original material, otherwise deformations in the joint would occur during the process. To inspect the hardness profile of the heat affected zone (HAZ), a set of indents (POLDI 568 01, Meopta, Czech Republic) in accordance with the Vickers hardness test method were performed (see Figure 5). Before the indentation, it was necessary to prepare the measured surface. To achieve a suitable surface roughness, the polishing procedure described in'Monitoring of material surface polishing procedure using confocal microscope' was applied [17]. This procedure was consistent with the surface preparation procedure specified by the technology provider.

3.5. SEM analysis

Before the scanning procedure, it was necessary to prepare the sample. A block of the sample with dimensions of $20 \times 200 \times 40$ mm was cut from the profile. The surface of the sample was polished using a diamond abrasive with a grain size of 3 μm to achieve the proper surface for etching with 5% nitric acid and alcohol (Nital). After the etching process (approx. 2 minutes), the Nital was cleaned off with alcohol and then dried. The Nital etching procedure was necessary to reveal the grain boundaries on the polished surface.

Scanning electron microscope (SEM) analyses (Jeol JSM-IT200 and TESCAN MIRA II LMU) were employed to reveal the phase changes in the structure, map the thermally affected area in detail, investigate the weld-base metal interface and perform a chemical analysis of the material with an Energy-dispersive detector (EDS) detector.

Figure 5. Hardness assembly using the Meopta Vickers apparatus on the HEB 140 profile.

4. Results and Discussion

4.1. Strain gauge measurement

The time-strain dependencies evaluated based on the values measured by the individual SGs show a certain trend with regards to the symmetrically placed strain gauges.

Point A indicates the deformation peak at the end of the pre-heating, point B corresponds to the time when the AT reaction was completed which means that the liquid metal is in weld form. Point C represents the strain values obtained at the time of the maximum heat input (measured using thermal imaging, see Figure 8). It is also possible to see the symmetry of the curves between the SG locations along the profile, thus it can be discussed that the magnitude and direction of the curves is affected by the shape and thickness of the profile. Some SGs become defective due to the high temperatures at which they were exposed to or from the epoxy peeling off the sample. Using a capsule SGs, attached by spot welding, would increase the resistance to high temperatures, but their high cost and greater difficulty in mounting them must be considered.

4.2. Optical measurement

The captured images, in combination with the DIC technique, allow one to determine the displacement/strain field or established set of the 'virtual' SGs on the surface of the sample. This strain evaluation technique is non-contact, which is beneficial with regards to the SG failure due to the high temperatures on the surface of profile. In the case of the performed experiments, five sub-areas were selected in the image of the surface of the observed sample. In each sub-area, four correlation points (placed in the corner) were tracked through the image sequence to determine the in-plane displacement vector. The calculated displacement values of all the correlation points in each sub-area were averaged to obtain statistically significant values. The resulting time-vertical/horizontal displacement dependencies evaluated using the DIC technique are shown in Figures 6 and 7. The individual curves indicate the displacement horizontally up

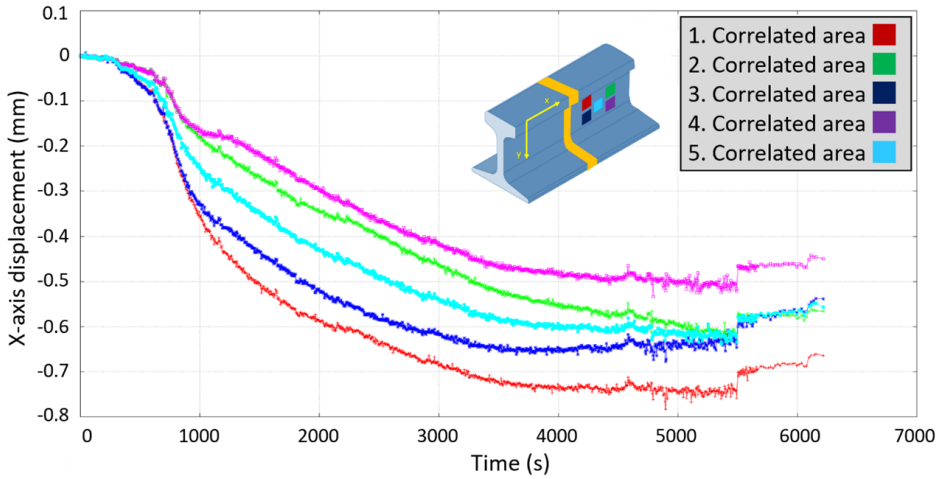

FIGURE 6. Comparison of the average values of the horizontal displacement of the individual correlation sub-areas.

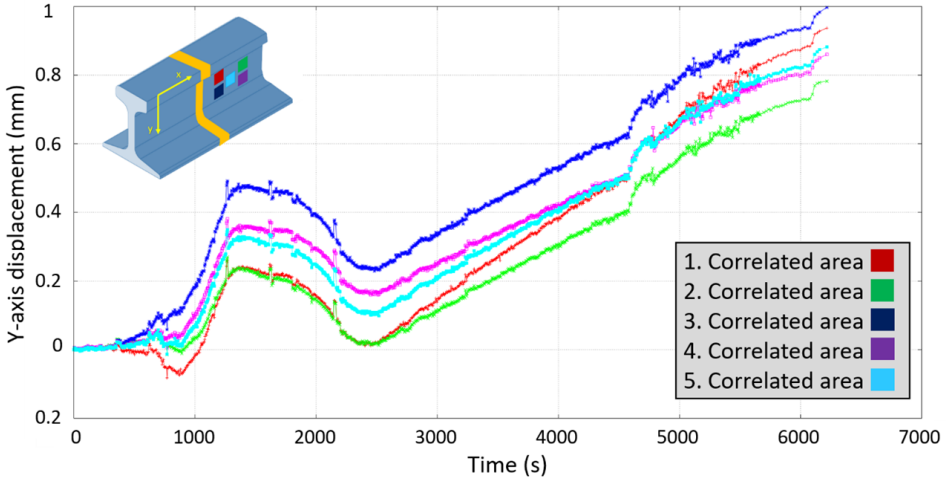

FIGURE 7. Comparison of the average values of the vertical displacement of the individual correlation sub-areas.

and vertically down the weld axis, the thermal dilation can be calculated from the data and the curves matched the trend from the thermographic camera recording. The different heights of the curves are caused by the different amount of heat input as each correlation area is at a different distance from the weld. Therefore, the closer the correlation area is to the weld, the values of the horizontal displacement are higher.

4.3. THERMOGRAPHIC MEASUREMENT

The AT reaction was monitored by a thermal imaging camera to achieve the distribution of the thermal field across the welded profile. Due to the technical limitations of the thermal imaging camera (temperature measurability up to 300 °C), the positions of the 'virtual' thermal measurement points had to be selected from the thermal field according to this limitation. The positions of the thermal measurement points were selected to be at a distance of 240 to 270 mm from the weld axis on both sides of the profile (see the scheme in Figure 8). Similar to the SG technological limitations for high temperatures, the thermal imaging camera is designed for a maximum temperature of 300 °C. For safe measurement, a maximum temperature of 200 °C was established which corresponds to the mentioned distances, which were calculated from knowledge of the heat propagation in the temperature courses observed in [18]. In the thermographic record, shown in Figure 8, the effect from the pre-heating and AT reaction (two peaks at approx. 600 seconds) and the subsequent heat input can be observed.

The trend of the thermographic curves of the HEB140 profile is similar to the trend of the 60E2 profile. As the HEB140 profile differs in thickness, the trend is slightly shifted.

4.4. PROFILE MEASUREMENT

The geometry of the plane of the running surface was measured after the metal had cooled. The so-called settlement of the weld after hot grinding has a trend according to the temperature of the material. The higher the temperature, the longer the time is required

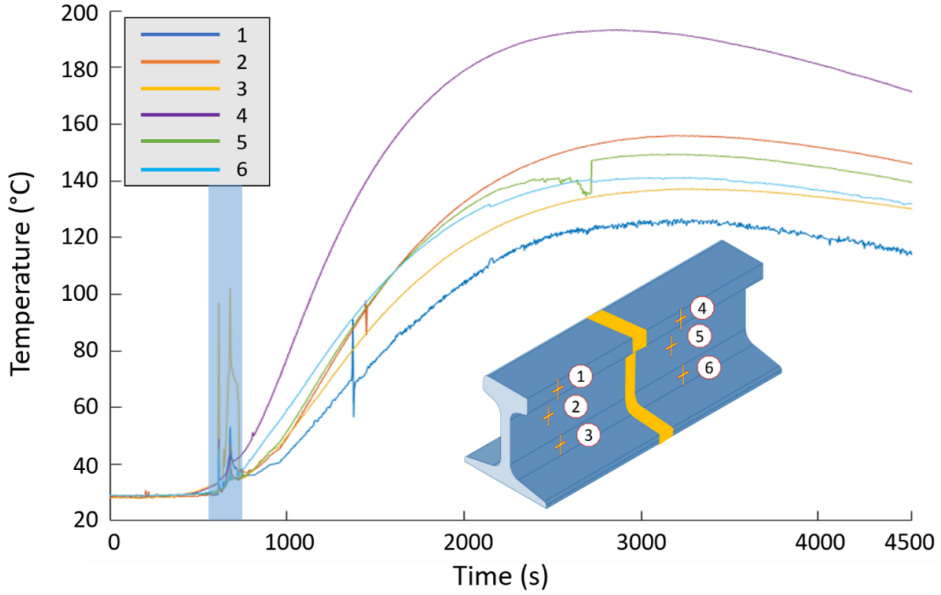

Figure 8. Thermographic record of the temperature profile for the 60E2 profile. The blue zone describes the effect from the pre-heating and AT reaction (500–700 seconds).

to correct the geometry. This measurement confirms the flatness guarantee provided by the manufacturer when following the technological procedure for the hot grinding of the weld metal. The tolerance for the flatness of a quarter of a metre from the weld axis on each side is ±0.5 mm. The plotted lines of the height profile in 2D show differences of up to 0.2 mm (see Figure 9 and Figure 10) and these differences are within the required limit. The same measurement was performed for the HEB140 profile, where the results were similar and also satisfy the prescribed tolerance.

4.5. Hardness measurement

In contrast to the other welding methods, where the weld hardness is lower than the original material, in the case of the AT reaction, the hardness of the resulting weld is higher than the hardness of the original material. Simultaneously, there is a HAZ issue that can be mitigated or eliminated by tempering during cooling. Due to the higher hardness, there is not an increase in the deformation under the action of operating loads and, thus, there is not any reduction in the service life. Figure 11 shows the hardness measurement performed on the running surface of the welded joints.

4.6. SEM analysis

The sample was etched and analysed using the Secondary Electron, Back-scattered Electron (SE, BSE) and EDS detectors. However, only SE images are presented due to the significant appearance of the surface (Figure 12). To examine the surface, the grain sizes of each metal phase and the elemental composition the SE images were sufficient. The investigation indicated lamellar cementite with a perlitic structure of the weld and base material, with different grain sizes corresponding to the introduced temperature. In addition, a softened area (i.e., the HAZ) with a spherical configuration of lamellar cementite can be observed and all the results were compared with the findings published in [18]. This configuration creates a thermally softened zone, which is a major issue in general welding.

5. Conclusion

The aim of this study was to evaluate the different experimental methods used to assess the progress of the AT reaction. The work provides background knowledge for further improvement of the experimental methods, which pushes the design limits. The used experimental methods allowed us to confirm the existence and the rate of the processes that take place during the AT welding. The processes that are known from theory have been demonstrated and their magnitude determined. On the basis of the thermography imaging, it was possible to show the rate of the thermal influence and the maximum temperature at various locations of the profile. This temperature field caused the thermal expansion observed by both strain evaluation methods, i.e., the SGs and the DIC method. The welding process affected the structure of the metal not only at the weld location, but also in the surrounding area. This finding was demonstrated both by measuring the hardness as a quantity involving the influence of processing and the "history" of the material and by studying the microstructure revealed by the SEM. The fact that AT welding, despite its turbulent nature, is a technologically mastered process was also confirmed by laser profilometry, which showed a very precise connection of the welded parts. The results and findings suggest the idea of repairing titanium alloy beams, either main or auxiliary ones, which form the airframe

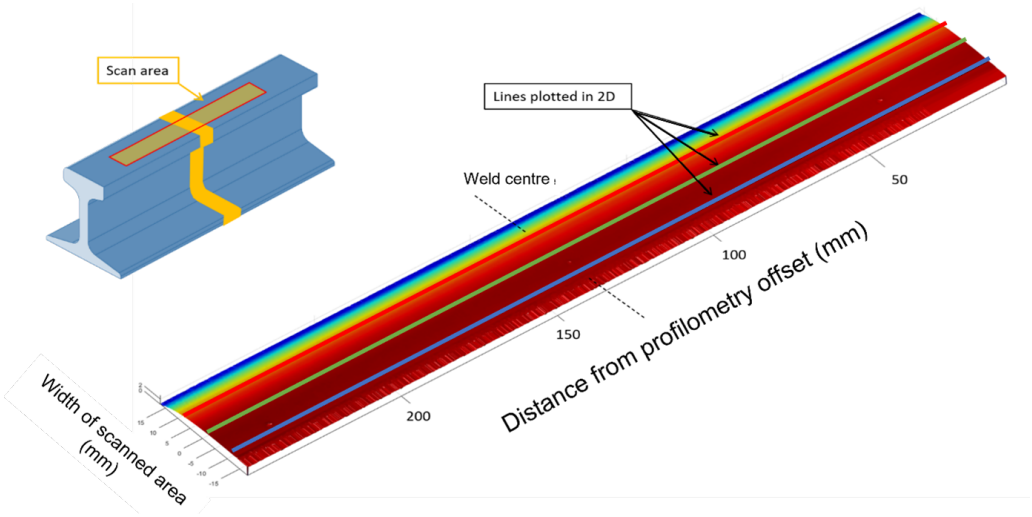

FIGURE 9. Height profile in 3D determined using the laser scanning technique. The colour scale indicates the height level, the edge of the profile has a radius, thus causing the colour transition. However, the plane along the profile is unchanged by the colour scale, this indicates a surface without roughness.

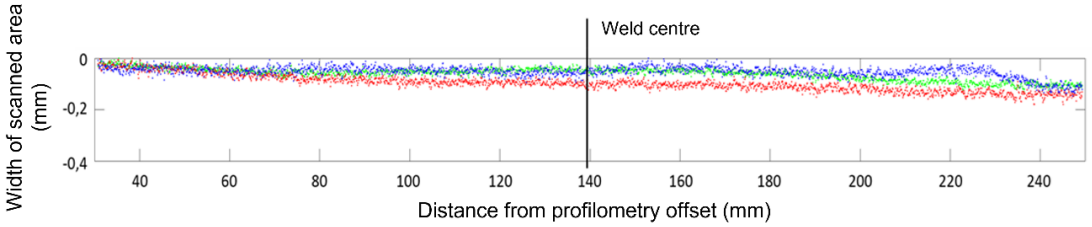

FIGURE 10. Height profile in 2D determined using laser scanning technique.

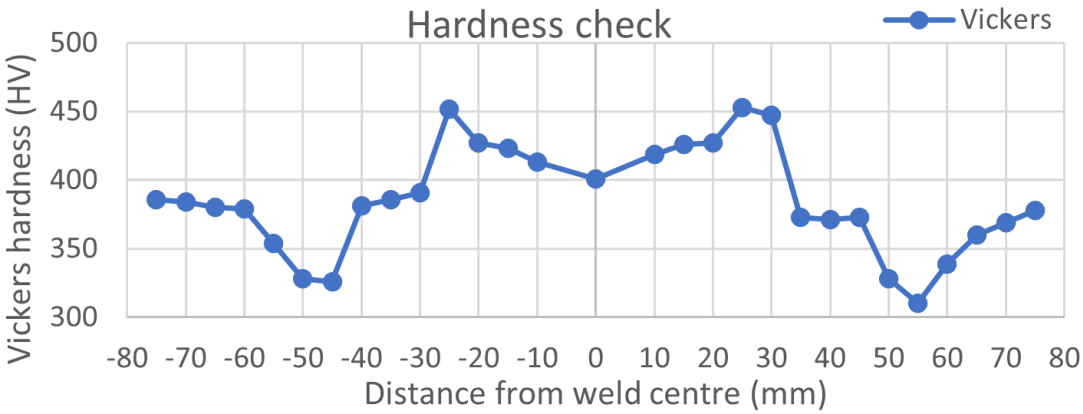

FIGURE 11. Hardness measurement of the running surface of the welded joints.

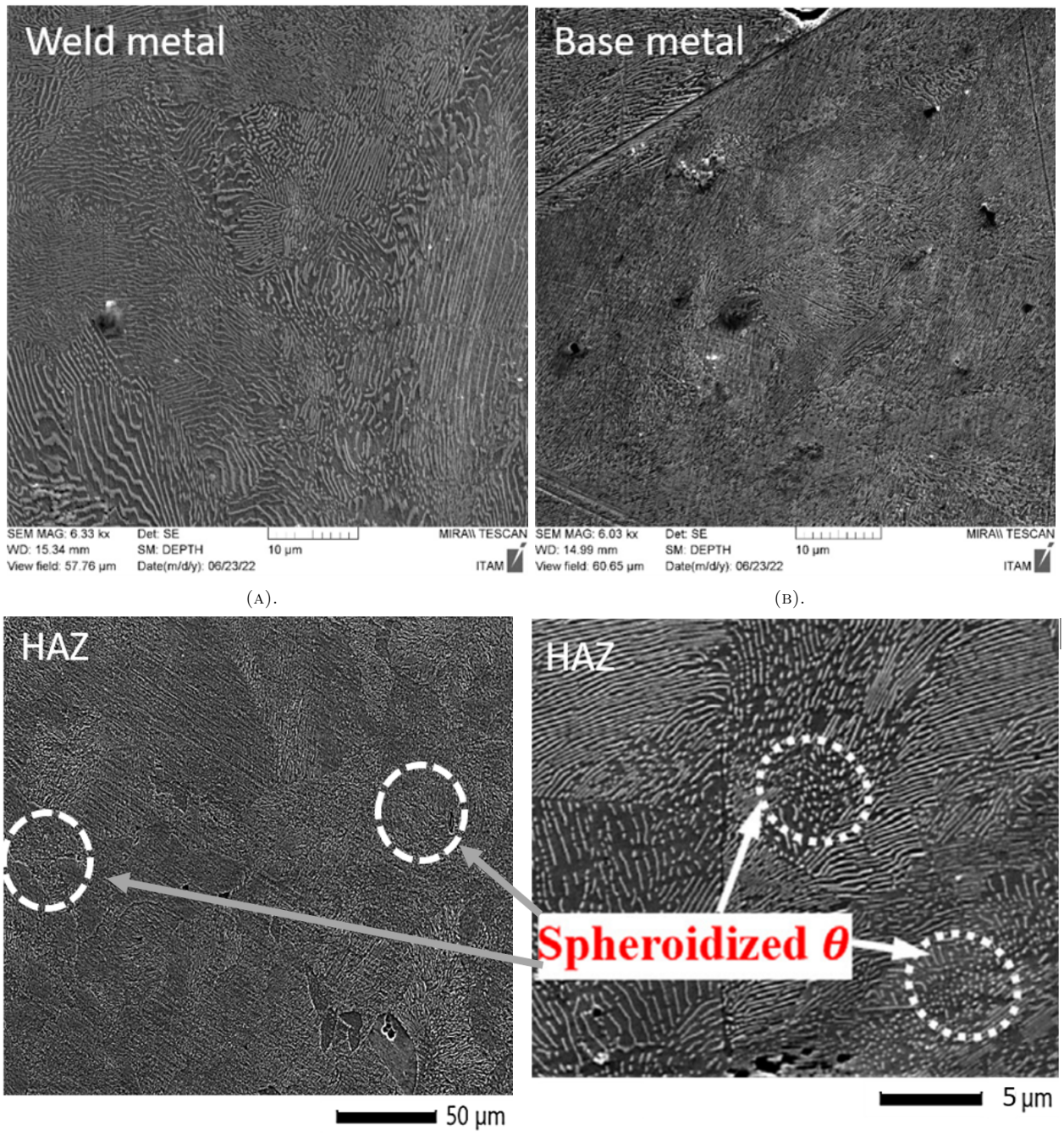

(A). (B). (C).

Figure 12. SEM analysis: the weld metal includes a larger grain than the base metal with cementite lamellae (top images), HAZ – spherical configuration of the cementite lamellae compared with the literature [18] (bottom images).

structure, using the AT reaction method is possible. This idea is supported by the possibility of the titanium alloy preparation introduced in [19]. Moreover, there is another important advantage with regards to the significant reduction in the human factor in the welding process. The application of this method would lead to a relatively fast repair of a deformed aircraft beam by cutting off the damaged part and replacing the new one with a welded joint. Another reason to use this method is the disadvantage of the existing rivet joints which is due to the rivet holes that are the initiators of cracks and directly affect the durability and reliability of the structures.

References

[1] P. Mendez, T. Eagar. New trends in weldind in the aeronautic industry. In *2nd Conference of New Manufacturing Trends*. 2002.

[2] H. B. Cary. *Modern Welding Technology Second Edition*. Prentice-Hall, Inc., 1988.

[3] H. Goldschmidt, C. Vautin. Aluminium as a heating and reducing agent. *The Journal of the Society of Chemical Industry* **6**(17):543–545, 1898.

[4] S. Kuchuk-Iatsenko, V. Cherednichok, L. Semenov. The flash-butt welding of aluminium alloys. *Welding in space and the construction of space vehicles by welding* pp. 198–208, 1991.

[5] K. Masubuchi. Integration of NASA-sponsored studies on aluminum welding. Tech. rep., NASA, 1972.

[6] O. Obeid, A. J. Leslie, A. G. Olabi. Influence of girth welding material on thermal and residual stress fields in welded lined pipes. *International Journal of Pressure Vessels and Piping* **200**:104777, 2022. https://doi.org/10.1016/j.ijpvp.2022.104777

[7] Y. Pang, N. Grilli, H. Su, et al. Experimental investigation on microstructures and mechanical properties of PG4 flash-butt rail welds. *Engineering Failure Analysis* **141**:106650, 2022. https://doi.org/10.1016/j.engfailanal.2022.106650

[8] M. Palaninatharaja, S. Julius Fusic, S. Karthikeyan, H. Ramesh. Automated vision system to measure weld length of hand brake. In *Advances in Lightweight Materials and Structures: Select Proceedings of ICALMS 2020*, pp. 175–185. Springer, 2020. https://doi.org/10.1007/978-981-15-7827-4_17

[9] H. Yamagishi. Tensile strength and fracture morphology of Fe/Al solid-state bonding interface obtained by forge welding: Effect of oxide scale and estimation of the bond strength of each phase. *Metallurgical and Materials Transactions A* **53**(11):4064–4080, 2022. https://doi.org/10.1007/s11661-022-06816-w

[10] W. Abd-Elaziem, M. Khedr, M. Newishy, H. Abdel-Aleem. Metallurgical characterization of a failed A106 Gr-B carbon steel welded condensate pipeline in a petroleum refinery. *International Journal of Pressure Vessels and Piping* **200**:104843, 2022. https://doi.org/10.1016/j.ijpvp.2022.104843

[11] S. Brotman, M. Djafari Rouhani, S. Charlot, et al. A benchmark study of burning rate of selected thermites through an original gasless theoretical model. *Applied Sciences* **11**(14):6553, 2021. https://doi.org/10.3390/app11146553

[12] P. Szabó. Novelizace předpisu SŽDC S3/2 bezstyková kolej. In *17. konference Železniční dopravní cesta*, pp. 118–130. 2012.

[13] Pandrol Ltd. PLA process OMM: UK welding PLA process operations maintenance manual, 2019. [2022-12-01], https://www.pandrol.com/wp-content/uploads/2019/07/UK-Welding-PLA-Process-OMM-EN.pdf.

[14] B. Pan. Digital image correlation for surface deformation measurement: historical developments, recent advances and future goals. *Measurement Science and Technology* **29**(8):082001, 2018. https://doi.org/10.1088/1361-6501/aac55b

[15] N. Novak, D. Kytyr, V. Rada, et al. Compression behaviour of tpms-filled stainless steel tubes. *Materials Science and Engineering: A* **852**:143680, 2022. https://doi.org/10.1016/j.msea.2022.143680

[16] D. C. Liu, J. Nocedal. On the limited memory BFGS method for large scale optimization. *Mathematical programming* **45**(1-3):503–528, 1989. https://doi.org/10.1007/BF01589116

[17] M. Dudíková, D. Kytýř, T. Doktor, O. Jiroušek. Monitoring of material surface polishing procedure using confocal microscope. *Chemické listy* **105**:790, 2011.

[18] Y. Liu, K. S. Tsang, E. Tan Zhi'En, et al. Investigation on material characteristics and fatigue crack behavior of thermite welded rail joint. *Construction and Building Materials* **276**:122249, 2021. https://doi.org/10.1016/j.conbuildmat.2021.122249

[19] I. Sharma, S. Majumdar, S. Chakraborty, A. Suri. Aluminothermic preparation of Hf–Ta and Nb–10Hf–1Ti alloys and their characterization. *Journal of alloys and compounds* **350**(1-2):184–190, 2003. https://doi.org/10.1016/S0925-8388(02)00999-4